Relativistic investigation of nuclear surface properties

D. Von-Eiff, W. Stocker, and M. K. Weigel
Sektion Physik, Ludwig-Maximilians-Universität München,
Am Coulombwall 1, D-85748 Garching, Germany
(Received 24 February 1994)

Calculations for semi-infinite nuclear matter within the relativistic Hartree approximation have been performed utilizing the nonlinear σ-ω model. We investigate the structure of the nuclear surface, i.e., the surface energy and the surface thickness, in its dependence on the properties of uniform nuclear matter in a systematic manner. We establish criterions for the selection of a relativistic mean-field parametrization following from the experimentally well determined, nuclear surface properties. In this respect, we discuss some currently used parameter sets. In addition, the accuracy of the semiclassical Thomas-Fermi approximation compared with the fully quantal approach is investigated. We close with some studies on density distributions (skewness parameter, Friedel oscillations, and the influence of the spin-orbit potential) and the nuclear curvature energy.

PACS number(s): 21.60.−n, 21.90.+f, 21.65.+f

I. INTRODUCTION

The investigation of nuclear systems has shifted strongly towards a relativistic approach (see, for instance, Refs. [1,2]). The Walecka model (for a review, see Ref. [1]) and its extension by Boguta and Bodmer [3], who added cubic and quartic terms in the scalar field, have been widely and successfully used to describe the ground-state properties of spherical and axially symmetric deformed nuclei [4,6], hot nuclei [7], giant resonances [8], magnetic moments [9], scattering processes of nucleons on nuclei at intermediate energies [10], and dynamical calculations of nuclear collisions [11]. While all these applications of the relativistic approach are based on the mean-field (Hartree) approximation, more fundamental models, such as Dirac-Hartree-Fock [12] or Dirac-Brueckner-Hartree-Fock [13,14], along with more sophisticated Lagrangians, have been used to investigate the properties of infinite nuclear matter (INM). Finite nuclei calculations within the latter approach are extremely involved. To our knowledge, results exist only for ^{16}O and ^{40}Ca [15]. Alternatively, calculations with mean-field Lagrangians whose parameters are fitted to Dirac-Brueckner-Hartree-Fock saturation curves and/or self-energies by means of density-dependent coupling constants [16,17] or least-squares methods [18] have attracted increasing attention during the last few years. In this sense, they allow the investigation of the properties of realistic nucleon-nucleon potentials within the relativistic Hartree framework.

However, the number of experimental nuclear properties investigated within the relativistic field theory is so far considerably smaller than those investigated and successfully reproduced by conventional nonrelativistic Skyrme calculations. Among these experimental nuclear properties are the nuclear surface properties. Several authors extracted the nuclear surface-energy coefficient from relativistic mean-field (RMF) calculations by fitting a mass formula to a few finite nuclei results [19,22]. However, the appropriate way to investigate surface properties is to study semi-infinite nuclear matter (SINM). This schematic system, free of "contaminating" shell, curvature, and Coulomb effects, constitutes a convenient test bench for the nuclear surface, as INM does for the bulk properties, to which any realistic theory of nuclear forces should be subjected. Previous RMF calculations of SINM have been done on the basis of (i) the Thomas-Fermi approximation [3,23,24]; (ii) the extended Thomas-Fermi approximation [25,26]; and (iii) the Hartree approximation ([27]; in Ref. [3] Boguta and Bodmer were the first to analyze the properties of SINM within the relativistic Hartree approach but in an approximate manner, insofar as they use Dirac wave functions, which do not depend on the nucleonic spin orientation thereby averaging the spin-orbit contributions to zero). While in Ref. [27] Hartree calculations for SINM are presented with a special emphasis on an accurate treatment of the spin-orbit part, a *systematic analysis* of the dependence of nuclear surface properties on the properties of uniform nuclear matter is still lacking up to now. To do this within the nonlinear σ-ω model is the main purpose of this paper. Thus, additional criterions for corresponding RMF parametrizations are provided.

Along with the relativistic Hartree approximation (RHA) for the nuclear surface properties we performed the corresponding relativistic Thomas-Fermi (RTF) calculations which enable us to investigate the accuracy of the latter in the case of SINM.

In addition, we analyze the nuclear surface properties for some currently used parameter sets, namely, NL1 [5,6], NL-SH [28], and SMFT [18]. While NL1 and NL-SH were obtained from a fit to the masses of several nuclei, SMFT is based on a least-squares fit to the saturation curve and self-energies of the one-boson-exchange (OBE) potential B, treated within the relativistic Dirac-Brueckner-Hartree-Fock (RDBHF) method [29]. Hence, for the first time we are able to provide information on the nuclear surface properties following from a realistic

nucleon-nucleon potential.

The paper is organized as follows. In Sec. II we briefly recall some basic concepts and definitions concerning SINM. The effective Lagrangian governing the relativistic dynamics is given. Section III contains the results and their discussion. In this order we investigate the surface energy and surface thickness, compare semiclassical approximations with the Hartree approach, present the surface properties for some current RMF parametrizations, and add some remarks on density distributions (skewness parameter, Friedel oscillations, and the influence of the spin-orbit potential) and the nuclear curvature energy. Our conclusions are drawn in Sec. IV.

II. BASIC CONCEPTS AND DEFINITIONS

In the liquid droplet model formulated by Myers and Swiatecki [30] the total energy of a spherical nucleus is written as

$$E = a_v A + 4\pi \int_0^\infty dr\, r^2 \{\mathcal{E}(r) - a_v \rho(r)\} \quad , \tag{1}$$

where a_v is the energy per particle in INM, while $\mathcal{E}(r)$ and $\rho(r)$ are the local energy and particle densities, respectively. Starting from (1) and following the method described in Ref. [30], one obtains the macroscopic surface-energy coefficient in SINM:

$$a_{\rm sf} = 4\pi r_0^2 \int_{-\infty}^\infty dz \{\mathcal{E}(z) - a_v \rho(z)\} \tag{2}$$

The nuclear radius parameter is given by $r_0 = [3/(4\pi\rho_0)]^{1/3}$, whereas the limiting behavior of the one-dimensional SINM system is characterized by

$$\lim_{z\to\infty} \rho(z) = 0 \tag{3}$$

and

$$\lim_{z\to-\infty} \rho(z) = \rho_0 \quad , \tag{4}$$

where ρ_0 is the equilibrium (saturation) density of INM for the given force.

Furthermore, the geometrical properties of the nuclear surface can be described by moments of the surface distribution function [7,31,32]. Starting with the normalized density distribution

$$f(z) := \frac{\rho(z)}{\rho_0} \quad , \tag{5}$$

the corresponding surface distribution function is defined as

$$g(z) := -\frac{df(z)}{dz} \quad . \tag{6}$$

Its first moment

$$z_0 := \int_{-\infty}^\infty g(z)\, z\, dz \tag{7}$$

denotes the location of the equivalent sharp surface, i.e., the point on the z axis for which the integral over the normalized density distribution (5) equals the integral over the step function $\Theta(z_0 - z)$. z_0 corresponds to the equivalent sharp radius in the case of spherical nuclei (cf. Ref. [7]).

One can also extract from SINM calculations the so-called surface thickness t, here defined as the 90% - 10% falloff distance of the surface density.

Another quantity of interest is the third moment of $g(z)$, the so-called skewness parameter b_3:

$$b_3^3 := \int_{-\infty}^\infty g(z)\ (z - z_0)^3\ dz \quad . \tag{8}$$

It measures the asymmetry of the falloff of the density distribution in the surface region. For a Fermi distribution, this falloff is symmetric with respect to the point of inflection, i.e., $b_3 = 0$. A negative value of b_3 corresponds to a density distribution with a long shoulder, followed by a steep falloff. An opposite behavior of $\rho(z)$ is reflected by $b_3 > 0$.

By means of an expansion of the surface-energy coefficient (2) in terms of the curvature κ ($2/R$ for a sphere of radius R) one gets the following for the macroscopic curvature-energy coefficient [30]:

$$a_c := a_c^{\rm geo} + a_c^{\rm dyn} = 8\pi r_0 \left[\int_{-\infty}^\infty dz\, (z - z_0) \{\mathcal{E}(z) - a_v \rho(z)\} + \int_{-\infty}^\infty dz \frac{\partial \{\mathcal{E}(z) - a_v \rho(z)\}}{\partial \kappa}\bigg|_{\kappa=0} \right] \quad . \tag{9}$$

The macroscopic coefficients a_v, r_0, $a_{\rm sf}$, and a_c in Eqs. (1), (2), and (9) are familiar from droplet-model mass formulas [30,33], as is the parameter t, but we stress that their definition does not depend on the validity of this model. In particular, they are also valid within relativistic approaches. The same holds for the skewness parameter b_3 [Eq. (8)].

For the relativistic dynamics we use the standard (extended) Walecka model, given by the Lagrangian density [1,3] ($F_{\mu\nu} \equiv \partial_\mu \omega_\nu - \partial_\nu \omega_\mu$; $\vec{G}_{\mu\nu} \equiv \partial_\mu \vec{b}_\nu - \partial_\nu \vec{b}_\mu$, with $\vec{b}_\mu$ denoting an isovector):

$$\mathcal{L} = \bar{\psi}\left(i\gamma^\mu\partial_\mu - M + g_\sigma\varphi - g_\omega\gamma^\mu\omega_\mu - g_\varrho\gamma^\mu\vec{\tau}\cdot\vec{b}_\mu\right)\psi + \frac{1}{2}\left(\partial_\mu\varphi\partial^\mu\varphi - m_\sigma^2\varphi^2\right) + \frac{1}{2}m_\omega^2\omega_\mu\omega^\mu - \frac{1}{4}F_{\mu\nu}F^{\mu\nu}$$
$$+\frac{1}{2}m_\varrho^2\vec{b}_\mu\cdot\vec{b}^\mu - \frac{1}{4}\vec{G}_{\mu\nu}\cdot\vec{G}^{\mu\nu} - \frac{1}{3}Mb\left(g_\sigma\varphi\right)^3 - \frac{1}{4}c\left(g_\sigma\varphi\right)^4 \quad . \tag{10}$$

The last two terms describe the σ self-interactions. The ϱ meson does not contribute to the properties of symmetric INM and SINM within the RHA. We included it in Eq. (10) because it is of relevance in Sec. III C concerning the volume-symmetry energy of some current RMF parametrizations.

The treatment of SINM within the semiclassical RTF approach is well known [3,23,24]. The theoretical foundations for the fully quantal RHA calculations have been outlined in detail by Hofer and Stocker [27] and we refer the reader to this reference.

III. RESULTS AND DISCUSSION

SINM calculations have been performed for the nonlinear parameter sets listed in Table I. While the energy per particle and the density at saturation are fixed to $a_v = -15.75$ MeV and $\rho_0 = 0.16$ fm^{-3}, the ranges of variation for the effective Dirac mass M^* ($0.55 \leq M^*/M \leq 0.80$) and the incompressibility K (200 MeV $\leq K \leq$ 300 MeV) cover the commonly accepted values.

A. Surface energy and surface thickness

The results for $a_{\rm sf}$ and t are given in Fig. 1. Within the RHA, symmetric INM properties only depend on the ratios $C_i^2 = g_i^2\left(M/m_i\right)^2$, $i = \sigma, \omega$, with M and m_i the nucleon mass and the corresponding meson mass, respectively, and the nonlinear couplings b and c. In contrast, the nuclear surface properties, extracted from the one-dimensional SINM system, are governed by the meson couplings and masses separately. The mass of the ω meson is fixed to its physical value, i.e., $m_\omega = 783$ MeV. The σ meson is supposed to represent the exchange of a 2π resonance and its mass should lie between 400 and 600 MeV. For the purposes of this contribution it turned out to be sufficient to look at the range 400 MeV $\leq m_\sigma \leq$ 550 MeV.

The RHA results in Fig. 1 (solid symbols) show the following systematic trends: For given K and M^*/M, $a_{\rm sf}$ and t decrease with increasing scalar mass m_σ, which is more visible for small M^*/M. This qualitatively agrees with the results for finite nuclei found in Ref. [34]. For constant M^*/M and m_σ, the surface energy increases

TABLE I. Nonlinear parameter sets. The energy per nucleon and density at saturation are fixed at $a_v = -15.75$ MeV and $\rho_0 = 0.16$ fm^{-3}, respectively. The dimensionless coupling constants are $C_i^2 = g_i^2\left(M/m_i\right)^2$, $i = \sigma, \omega$, with the nucleon mass $M = 939$ MeV.

K [MeV]	M^*/M	C_ω^2	C_σ^2	$b \times 10^3$	$c \times 10^3$
200	0.55	246.481	369.156	2.363	−3.451
	0.60	216.215	335.467	2.907	−4.059
	0.65	185.491	303.338	3.892	−5.156
	0.70	154.393	272.305	5.643	−7.056
	0.75	122.985	242.116	8.833	−10.088
	0.80	91.319	211.908	14.616	−11.857
250	0.55	246.481	362.704	2.042	−2.975
	0.60	216.215	328.283	2.418	−3.245
	0.65	185.491	295.104	3.103	−3.656
	0.70	154.393	262.654	4.294	−4.057
	0.75	122.985	229.872	6.193	−3.047
	0.80	91.319	195.449	8.655	8.012
300	0.55	246.481	356.289	1.711	−2.485
	0.60	216.215	321.218	1.916	−2.408
	0.65	185.491	287.132	2.297	−2.118
	0.70	154.393	253.244	2.879	−0.914
	0.75	122.985	218.458	3.465	4.226
	0.80	91.319	179.961	2.050	30.030

with the incompressibility. Concerning the dependence of the surface thickness on K, one would intuitively expect t to decrease, i.e., a sharper nuclear surface, with increasing incompressibility. Such a behavior can be found for a scalar mass $m_\sigma = 400$ MeV as well as for the combinations ($m_\sigma = 450$ MeV, $M^*/M \leq 0.7$) and ($m_\sigma = 500$ MeV, $M^*/M \geq 0.7$). The remaining regions in the $m_\sigma - \frac{M^*}{M}$ plane show no systematic trends for t as a function of K. Looking at a_{sf} and t as a function of M^*/M with K and m_σ fixed, both quantities decrease with increasing M^*/M for $m_\sigma = 400$ and 450 MeV. For larger values of the scalar mass the surface energy shows a nonmonotonic behavior, more visible for $m_\sigma = 550$ MeV. The surface thickness still displays a decreasing trend with increasing M^*/M for $m_\sigma = 500$ MeV, but for the largest value of the σ-meson mass a nonmonotonic pattern, as for the surface energy, is visible.

Postulating the existence of an energy-density functional, an algebraic pocket formula was derived in Ref. [35] under some simplifying assumptions. It correlates the macroscopic surface parameters, the surface tension $\sigma = a_{sf}/4\pi r_0^2$ (i.e., the surface energy per unit area) and the surface thickness t, with the bulk parameters ρ_0 and K. From this formula the ratio σ/t turns out to be a function of K and ρ_0 alone, i.e., it is given by bulk properties. This leads to a qualitative understanding of the obvious parallel nature of corresponding curves in the upper and lower diagrams of Fig. 1.

The experimental regions for a_{sf} and t are indicated by the horizontal dashed lines in Fig 1. While the surface-energy coefficient should be around 16.5 and 21 MeV [27], the surface thickness is well determined by electron-scattering data [36,37] to lie in the range 2.35 ± 0.10 fm. Figure 1 shows that several nonlinear parametrizations are able to yield realistic values for the surface-energy coefficient a_{sf} and the surface thickness t separately. Demanding both, a_{sf} and t, to lie in the corresponding empirical region simultaneously, we found only two suitable parameter sets. These are the combinations ($K = 200$ MeV, $m_\sigma = 400$ MeV, $M^*/M = 0.75$) and ($K = 200$ MeV, $m_\sigma = 450$ MeV, $M^*/M = 0.70$) with the surface properties $a_{sf} = 20.54$ MeV, $t = 2.45$ fm and

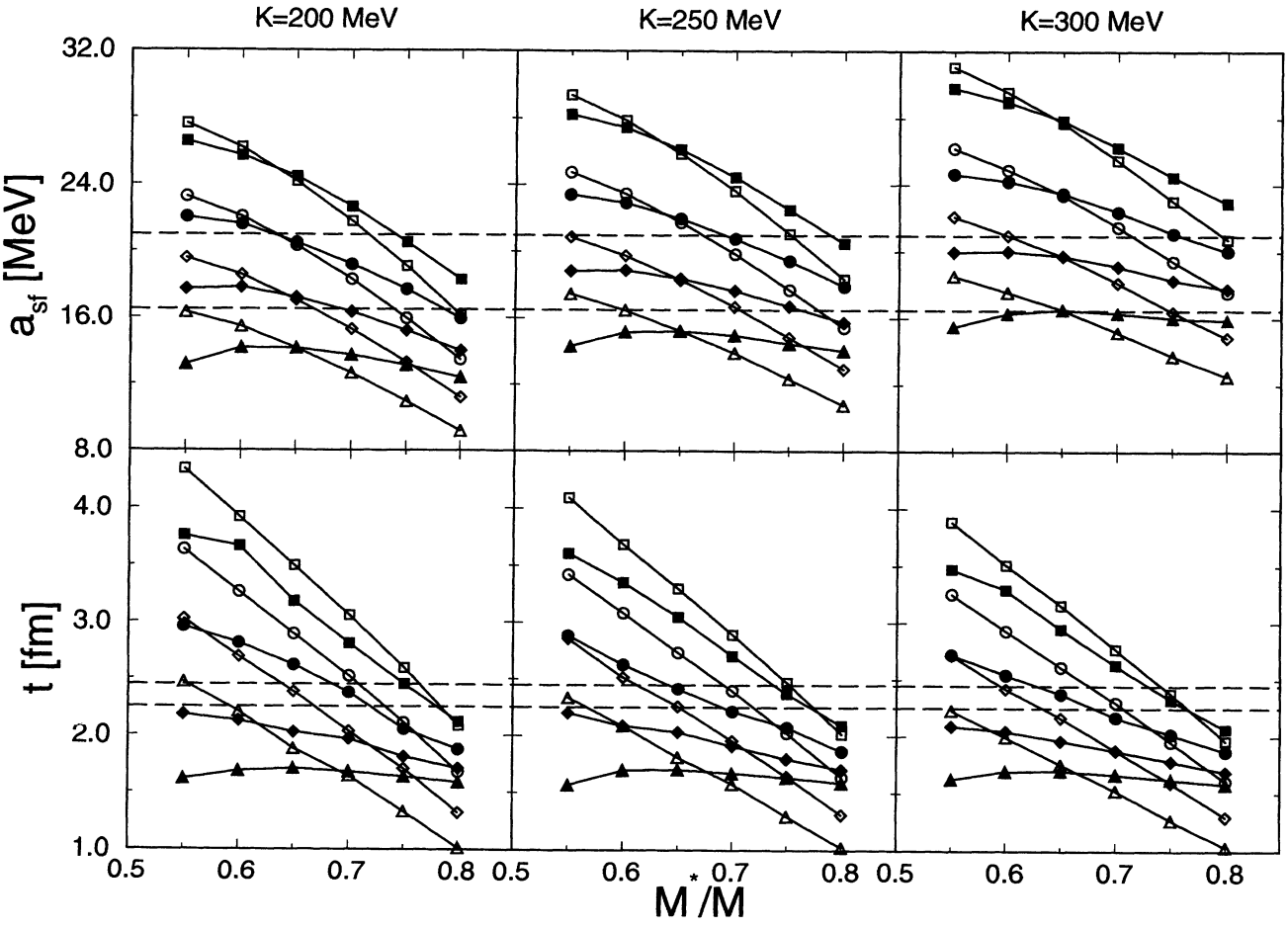

FIG. 1. Surface-energy coefficient a_{sf} and surface thickness t of semi-infinite nuclear matter calculated in the relativistic Hartree (solid symbols) and the relativistic Thomas-Fermi (empty symbols) approximation for the nonlinear parameter sets given in Table I. Squares, circles, diamonds, and triangles correspond to a scalar mass m_σ of 400, 450, 500, and 550 MeV, respectively. The dashed lines indicate the empirical regions. The solid lines connecting the symbols are to guide the eye.

$a_{sf} = 19.21$ MeV, $t = 2.38$ fm, respectively. Therefore we conclude that the nuclear surface properties strongly favor a nonlinear parametrization of the RMF theory with a *low incompressibility* ($K \approx 200$ MeV), a *small scalar mass* (400 MeV $\leq m_\sigma \leq$ 450 MeV), and a *high effective Dirac mass* ($0.70 \leq M^*/M \leq 0.75$). Especially the latter point raises a problem: The experimental spin-orbit splitting in light nuclei determines the effective Dirac mass within narrow limits to be around $M^*/M \approx 0.60$ [38]. Now the surface properties impose a second range for M^*/M. It seems that RMF theory with only four adjustable parameters possesses not enough degrees of freedom to accomplish all experimental demands simultaneously.

B. Semiclassical vs Hartree approach

As a byproduct, our calculations enable us to investigate the accuracy of the semiclassical RTF method compared with the fully quantal results for the surface properties. The RTF results for a_{sf} and t, calculated with the nonlinear sets of Table I, are displayed as empty symbols in Fig. 1. Concerning systematic trends, the semiclassical approach does not reflect the subtle effects of the RHA results as described above: The surface-energy coefficient a_{sf} and the surface thickness t decrease with increasing scalar mass and effective Dirac mass, a_{sf} increases with the incompressibility, and t decreases with increasing K (despite $m_\sigma = 550$ MeV and $M^*/M = 0.8$).

For low values of M^*/M the RTF approach overestimates the surface energy compared with the RHA results. This is better visible for large values of the scalar mass (for $M^*/M = 0.55$ deviations up to 23.7% for $m_\sigma = 550$ MeV, while for $m_\sigma = 400$ MeV the maximum relative discrepancy is 4.2%). Contrastly, for large effective Dirac masses a similar trend is visible (for $M^*/M = 0.8$ maximum relative discrepancies of 25.9% and 11.7% for $m_\sigma = 550$ and 400 MeV, respectively), but with the RTF approximation underestimating the fully quantal results for a_{sf} (in particular for small incompressibilities). Therefore, within the range $0.55 \leq M^*/M \leq 0.80$ a value for the effective Dirac mass can be found for which RTF and RHA surface-energy results coincide. For all values of K and m_σ that we considered, the best agreement between semiclassical and fully quantal results for a_{sf} occurs for $M^*/M = 0.65$. This perfectly agrees with what Centelles *et al.* [39] found for the total energies of finite nuclei.

Comparing RTF and RHA results for the surface thickness, one can find trends similar (though not as systematic) as those seen for the surface energy. Again, a m_σ-dependent overestimation of t by the semiclassical approach for small M^*/M (for $M^*/M = 0.55$ deviations up to 53.2% for $m_\sigma = 550$ MeV, while for $m_\sigma = 400$ MeV the maximum relative discrepancy is 15.6%) along with an underestimation for large effective Dirac masses (for $M^*/M = 0.8$ maximum relative discrepancies of 35.8% and 5.0% for $m_\sigma = 550$ and 400 MeV, respectively) can be stated. But in contrast to the surface energy, no unique value of M^*/M can be found for which the agreement between the two approaches is best. While for small values of K and m_σ this is the case for $M^*/M = 0.80$, increasing scalar mass and incompressibility shift the point of intersection between the semiclassical and fully quantal results for t towards smaller effective Dirac masses, ending up with $M^*/M = 0.65$ for the combination ($K = 300$ MeV, $m_\sigma = 550$ MeV).

Centelles and Viñas performed relativistic extended Thomas-Fermi (RETF) calculations for SINM [26]. The RETF approach improves the pure RTF method by inclusion of gradient corrections up to the order $\hbar^2$ by means of density-functional techniques. With the fully quantal RHA results available now, we are able to assess the quality of the RETF description of the nuclear surface in a systematic manner. The general trends of the RETF results for a_{sf} and t are comparable with those of the RTF approach as described above. In particular, the nonmonotonic RHA behavior of the nuclear surface properties with M^*/M for large scalar masses cannot be described within any of the semiclassical approximations, RTF and RETF. In contrast to the RTF approximation, the RETF approach underestimates the fully quantal results for a_{sf} and t for all values of M^*/M. This again is in agreement with the finite nuclei investigations of Ref. [39], where a general overbinding, independent on the effective Dirac mass, in RETF, compared with the RHA results, was observed. Concerning the quantitative agreement between the two approaches, a strong dependence on M^*/M and m_σ occurs: While for $m_\sigma \leq 450$ MeV the deviations of the RETF results from the fully quantal values are mostly less than 10%, the situation becomes worse for large scalar and effective Dirac masses. The maximum relative discrepancies that we found are 16.9% and 33.8% for a_{sf} and t, respectively ($K = 200$ MeV, $m_\sigma = 550$ MeV, $M^*/M = 0.80$). It should be mentioned that the convergence problems occurring in the RETF calculations for large scalar and small effective Dirac masses are not present within the fully quantal RHA. Nevertheless, with the RHA results as a reference, the RETF approach constitutes an improvement of the pure RTF method.

C. Surface properties for some current RMF parametrizations

We also investigated the surface properties for some current parameter sets, displayed in Table II. As mentioned above, NL1 [5,6] and NL-SH [28], the latter of which possesses more reasonable symmetry and surface-symmetry properties [24,28], were obtained from a fit to the masses of several nuclei. In Table III the corresponding INM and SINM properties are shown. For NL1 both, the surface-energy coefficient and surface thickness, agrees very well with experiment (the RTF [24] and RETF [26] results are $a_{sf} = 19.78$ MeV, $t = 2.90$ fm and $a_{sf} = 17.40$ MeV, $t = 2.09$ fm, respectively). This agreement might be surprising at the first sight in view of the above statement that, apart from a low incompressibility ($K \approx 200$ MeV), effective Dirac and scalar masses in the ranges $0.70 \leq M^*/M \leq 0.75$ and 400 MeV $\leq m_\sigma \leq$

TABLE II. Parameter sets NL1 [6], NL-SH [28], and SMFT [18] with the nucleon and meson masses given in MeV. $C_i^2 = g_i^2\,(M/m_i)^2$, $i = \sigma, \omega, \varrho$.

	NL1	NL-SH	SMFT
M	938.000	939.000	938.926
m_σ	492.250	526.059	550.000
m_ω	795.360	783.000	782.600
m_ϱ	763.000	763.000	
C_σ^2	373.176	347.533	282.899
C_ω^2	245.458	240.997	179.880
C_ϱ^2	37.4175	29.0954	
$b \times 10^3$	2.4578	1.2747	3.3110
$c \times 10^3$	−3.4334	−1.3308	−4.3120

450 MeV, respectively, are necessary to achieve a simultaneous agreement of $a_{\rm sf}$ and t with experiment. Indeed, for the combination (K = 200 MeV, m_σ = 500 MeV, $M^*/M = 0.55$), which comes closest to the corresponding NL1-values, we found (cf. Fig. 1) $a_{\rm sf}$ = 17.70 MeV and t = 2.18 fm. But in contrast to the calculations underlying Fig. 1, for which the mass of the ω meson was fixed to its empirical value m_ω = 783 MeV, NL1 has a higher value for m_ω (cf. Table II). Within RMF theory for symmetric SINM the ω-meson contribution, whose range is determined by m_ω, represents the entire repulsive part of the nuclear potential. Intuitively, a larger m_ω, i.e., a shorter range of the repulsive part of the nuclear potential, with the range of its attractive counterpart, determined by m_σ, unchanged, should have the same net effect as a decreasing scalar mass, i.e., a less steep nuclear surface. This expectation is confirmed by the NL1 surface properties. Coming back to the above statement concerning the number of degrees of freedom in RMF theory, one clearly sees that with the ω-meson mass as an additional adjustable parameter, the experimental requirements for the spin-orbit splitting ($M^*/M \approx 0.6$) and the surface properties can be accomplished simultaneously.

In contrast, NL-SH contains the physical value for m_ω, and its surface properties behave as one would expect from the systematic analysis presented above: While the surface energy lies in the empirical region, the surface thickness is much too small compared with experiment (the RTF [24] results are $a_{\rm sf}$ = 20.07 MeV and t = 2.09 fm).

The set SMFT in Table II was obtained by a least-squares fit of the parameters C_σ^2, C_ω^2, b, and c to the saturation curve and self-energies of the OBE potential B [29], with the nucleon and meson masses fixed to the corresponding realistic values. Since within RMF theory, the ϱ meson does not contribute to the properties of symmetric INM (nor to those of symmetric SINM), the ϱ-nucleon coupling had not to be fitted. Therefore, the small value for the SMFT volume-symmetry energy, a_4, in Table III contains only the "kinetic" part. Taking the values of the OBE potential B [29], i.e., m_ϱ = 769 MeV and C_ϱ^2 = 17.7969, for the mass and the coupling of the ϱ meson, respectively, one finds, in very good agreement with the experiment, a_4 = 30.06 MeV.

By means of this RMF parametrization of the OBE potential B we are for the first time able to provide information on the nuclear surface properties of a realistic nucleon-nucleon potential. The results for $a_{\rm sf}$ and t in Table III fit into the systematic scheme described above. Neither the surface energy nor the surface thickness lies in the empirical range; both values are much too small compared with experiment. The corresponding RTF results are $a_{\rm sf}$ = 14.47 MeV and t = 2.02 fm (as described above, the SMFT value for the effective Dirac mass, $M^*/M = 0.655$, ensures that RTF calculations for the surface energy and total energies of finite nuclei [39] provide a very good estimation of the corresponding RHA results).

D. Density distributions and curvature energy

In considering the RHA density distributions, two effects have to be discussed, namely, Friedel oscillations and spin-orbit effects.

The nuclear densities and meson fields oscillate as a function of z with a wavelength of π/k_F [$k_F = (3\pi^2\rho_0/2)^{\frac{1}{3}}$] and amplitudes falling off with the inverse of the distance from the surface. These so-called Friedel oscillations are discussed for the nonrelativistic case in detail in Ref. [40]. Within the relativistic σ-ω model such oscillations have been investigated in connection with the so-called Overhauser effect [41]. In any case, Friedel oscillations are a typical surface effect and the

TABLE III. Properties of infinite nuclear matter (energy per particle a_v, density ρ_0, incompressibility K, effective Dirac mass M^*/M, and volume symmetry energy a_4 at saturation) and semi-infinite nuclear matter (surface-energy coefficient $a_{\rm sf}$ and surface thickness t) for the parameter sets NL1, NL-SH, and SMFT (see text).

Set	a_v [MeV]	ρ_0 [fm^{-3}]	K [MeV]	M^*/M	a_4 [MeV]	$a_{\rm sf}$ [MeV]	t [fm]
NL1	−16.423	0.1519	211.7	0.573	43.49	18.56	2.30
NL-SH	−16.346	0.1460	355.8	0.597	36.13	18.96	1.83
SMFT	−13.851	0.1629	212.4	0.655	17.43	14.39	1.83

SINM model system provides an appropriate framework for their study.

In Fig. 2 we plotted the total nucleon density for various values of the effective Dirac mass whereas the incompressibility and the scalar mass are fixed to $K = 250$ MeV and $m_\sigma = 400$ MeV, respectively. As we know from Sec. III A, for such a σ-meson mass the surface thickness t strongly decreases with increasing M^*/M (cf. Fig. 1). This is clearly visible in Fig. 2. At the same time Friedel oscillations appear with increasing effective Dirac mass, i.e., small values for t. For low values of M^*/M, i.e., a large surface thickness, there is no opportunity for these oscillations to be built up.

A second remarkable effect is the impact of the spin-orbit force on the density distributions. For the strength of the effective single-particle spin-orbit potential in symmetric SINM one gets an expression [27], that in the Foldy-Wouthuysen approximation is given by

$$W(z) = \frac{1}{4M^2}\left(g_\omega \frac{d\omega_0(z)}{dz} + g_\sigma \frac{d\varphi(z)}{dz}\right) \quad , \qquad (11)$$

where $g_\omega\omega_0(z)$ and $g_\sigma\varphi(z)$ denote the timelike and the scalar self-energy component within the RHA, respectively. It was found in Ref. [27] that $W(z)$ strongly increases with m_σ. This is in agreement with Sec. III A: The surface thickness decreases with increasing scalar mass (cf. Fig. 1). Hence, a steeper falloff of the meson fields and in turn a larger spin-orbit strength (11) is expected (compare also Ref. [34] for the case of spherical nuclei).

Furthermore, the spin-orbit potential is attractive for particles with the spin orientation $\lambda = +1$ and repulsive for those with $\lambda = -1$, resulting in a depletion of $\lambda = -1$ particles in the surface ([27]; for the nonrelativistic case see also Ref. [42]). If the strenght of the spin-orbit potential is large, i.e., m_σ is large (see above), attraction dominates over repulsion and the total nucleon density $\rho(z)$ displays an enhancement in the surface region, though we are investigating a spin saturated system, i.e., there is no resultant spin. This is illustrated in Fig. 3, where we plotted for the various values of m_σ the total nucleon density $\rho(z) = \rho^+(z) + \rho^-(z)$ along with the corresponding contributions for the different spin orientations $\lambda = \pm 1$. With increasing scalar mass one gets both, Friedel oscillations and the spin-orbit effect described above. For $m_\sigma = 550$ MeV they are abruptly adding up to the remarkable increase of $\rho(z)$ in the surface region (compare Fig. 4 of Ref. [27] where both effects are investigated separately). Looking at the surface thickness, $t = 3.61$, 2.88, 2.20, and 1.57 fm for $m_\sigma = 400$, 450, 500, and 550 MeV, respectively. Hence, for a realistic value of t such an enhancement does not occur.

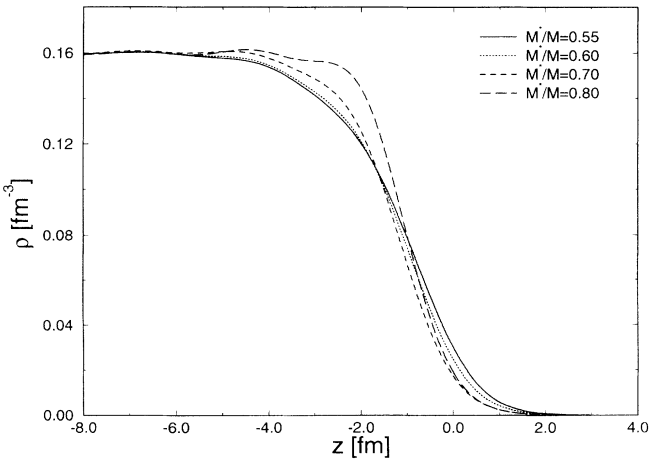

FIG. 2. Density distributions for various values of M^*/M. The incompressibility and the scalar mass are fixed to $K = 250$ MeV and $m_\sigma = 400$ MeV, respectively.

For the reasons described above, namely, the influence of Friedel oscillations and spin-orbit effects on nuclear density distributions, the problem of an exact and numerically reliable determination of the surface distribution function $g(z)$ [Eq. (6)] and in turn of z_0 [Eq. (7)] arises (of course, such difficulties are present also within the nonrelativistic scheme; see Ref. [43] and references therein). Therefore, as a first step, we calculated the skewness parameter b_3 and the geometrical part of the curvature-energy coefficient $a_c^{\rm geo}$ [Eqs. (8) and (9), respectively], both of which sensitively depend on the location of the equivalent sharp surface, only for such cases where the above problems do not occur, i.e., for parameter sets with $M^*/M = 0.55$ and $m_\sigma = 400$ MeV (cf. Figs. 2 and 3). The corresponding results, together with the RTF values for which the problems of Friedel oscillations and spin-orbit effects do not exist, are presented in Table IV.

For both, the RHA and RTF approaches, the dependence of the skewness parameter on the incompressibility is not that strong, showing an increasing behavior with increasing K. Of greater importance is the fact, that the absolute RTF values for b_3 exceed the corresponding RHA results by more than 50%. As described in Sec. II, this corresponds to typical semiclassical density distributions with too long a shoulder, followed by too steep a falloff compared with fully quantal density distributions.

Before discussing the results for the curvature-energy coefficient a_c, some remarks are necessary. The two contributions of Eq. (9) are called geometrical and dynamical, respectively. The geometrical part describes the

TABLE IV. Skewness parameter b_3 and the geometrical part of the curvature-energy coefficient $a_c^{\rm geo}$ (see text) within the RHA and RTF approaches for the values of the incompressibility considered in this paper. The effective Dirac and the scalar mass are fixed to $M^*/M = 0.55$ and $m_\sigma = 400$ MeV, respectively. For $a_c^{\rm geo}$ we also included RETF results available from Ref. [26].

K [MeV]	b_3 [fm]		$a_c^{\rm geo}$ [MeV]		
	RHA	RTF	RHA	RTF	RETF [26]
200	−1.16	−1.77	13.87	28.56	30
250	−1.09	−1.69	12.70	27.57	
300	−1.07	−1.62	12.15	26.98	26.5

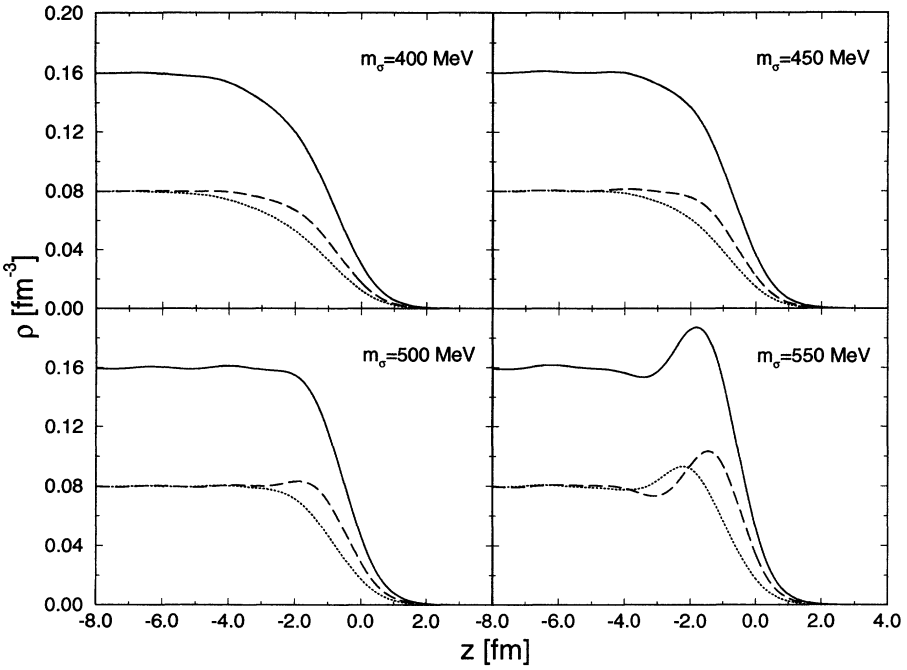

FIG. 3. Total nucleon density $\rho(z) = \rho^+(z) + \rho^-(z)$ (solid lines) together with the corresponding contributions $\rho^+(z)$ (long-dash lines) and $\rho^-(z)$ (dotted lines) for the different spin orientations $\lambda = \pm 1$, respectively (cf. Refs. [27,42]). The various values of the scalar mass m_σ correspond to different surface thicknesses (see text). The incompressibility and the effective Dirac mass are fixed to $K = 250$ MeV and $M^*/M = 0.55$, respectively.

variation of the surface-energy density, $\mathcal{E}(z) - a_v\rho(z)$, across the surface parallel to the z axis. This part is affected by the problem described above concerning the exact determination of z_0. As for the skewness parameter, we restrict ourselves to parameter sets ($M^*/M = 0.55$, $m_\sigma = 400$ MeV) for which reliable results can be expected.

For the evaluation of the dynamical part $a_c^{\rm dyn}$ one needs the energy density $\mathcal{E}(z)$ as an explicit functional of all gradient contributions to extract the curvature-dependent parts. Such a procedure is possible within a semiclassical framework where the energy-density functional is known (see, for instance, Ref. [44]). The extraction of the explicit κ dependence of $\mathcal{E}(z)$ within the RHA is a nontrivial problem which has not been solved yet. As in past calculations, we therefore restricted our calculations to the geometrical part $a_c^{\rm geo}$. This also holds for the RETF results of Ref. [26] (we extracted the corresponding values from Fig. 3 of this reference).

The geometrical part $a_c^{\rm geo}$ decreases with increasing incompressibility. However, the dependence on K is not that strong within both semiclassical and fully quantal approaches. In comparing the semiclassical results with the RHA values, there is a striking disagreement.

Compared with the empirical value ($a_c \approx 0$ MeV) our RHA results for $a_c^{\rm geo}$ fit into the trend of all past (relativistic and nonrelativistic) calculations, which report a curvature energy much too large (of the order of 10 MeV; Refs. [26,43,44], and references therein).

IV. SUMMARY AND CONCLUSIONS

To summarize, we present a systematic analysis of nuclear surface properties within the relativistic Hartree approximation. Using the nonlinear RMF parametrization, which allows one to cover the commonly accepted ranges for the incompressibility and effective Dirac mass, we find the nuclear surface properties to strongly favor parametrizations with a *low incompressibility* ($K \approx$ 200 MeV), a *small scalar mass* (400 MeV $\leq m_\sigma \leq$ 450 MeV), and a *high effective Dirac mass* ($0.70 \leq M^*/M \leq 0.75$). The latter point especially, not in full agreement with the requirements for a correct spin-orbit splitting, indicates that the phenomenological RMF theory with five adjustable parameters (including the scalar mass) does not possess enough degrees of freedom to accomplish all experimental demands simultaneously. In addition, we performed semiclassical RTF calculations which over (under) estimate the fully quantal results for the surface energy and thickness at low (high) effective Dirac masses. For $M^*/M = 0.65$ a very good agreement for the surface energy within RHA and RTF approaches can be achieved. The surface properties for some currently used parameter sets are investigated. In particular, for the first time information on the nuclear surface properties of a realistic nucleon-nucleon potential is available. Finally, some studies on density distributions (skewness parameter, Friedel oscillations, and the influence of the spin-orbit potential) and the nuclear curvature energy are presented. The results concerning the latter indicate that for such a subtle quantity, semiclassical approaches might not be sufficient within the relativistic framework.

ACKNOWLEDGMENTS

We would like to thank J. Ramschütz for providing his numerical codes for symmetric infinite nuclear matter. The authors wish to thank J. M. Pearson for stimulating discussions. D. V.-E. acknowledges the financial support of the Deutsche Forschungsgemeinschaft (DFG).

[1] B.D. Serot and J.D. Walecka, in *Advances in Nuclear Physics*, edited by J.W. Negele and E. Vogt (Plenum, New York, 1986), Vol. 16.
[2] L.S. Celenza and C.M. Shakin, in *Relativistic Nuclear Physics*, Lecture Notes in Physics Vol. 2 (World Scientific, Singapore, 1986).
[3] J. Boguta and A.R. Bodmer, Nucl. Phys. **A292**, 413 (1977).
[4] R.J. Furnstahl, C.E. Price, and G.E. Walker, Phys. Rev. C **36**, 2590 (1987).
[5] P.-G. Reinhard, Rep. Prog. Phys. **52**, 439 (1989), and references therein.
[6] Y.K. Gambhir, P. Ring, and A. Thimet, Ann. Phys. (N.Y.) **198**, 132 (1990).
[7] D. Von-Eiff and M.K. Weigel, Phys. Rev. C **46**, 1288 (1992).
[8] H.F. Boersma, R. Malfliet, and O. Scholten, Phys. Lett. B **269**, 1 (1991).
[9] U. Hofmann and P. Ring, Phys. Lett. B **214**, 307 (1988).
[10] B.C. Clark, S. Hama, R.L. Mercer, L. Ray, and B.D. Serot, Phys. Rev. Lett. **50**, 1644 (1983).
[11] R.Y. Cusson, P.-G. Reinhard, J.J. Molitoris, H. Stöcker, M.R. Strayer, and W. Greiner, Phys. Rev. Lett. **55**, 2786 (1985).
[12] P. Bernardos, V.N. Fomenko, Nguyen Van Giai, M.L. Quelle, S. Marcos, R. Niembro, and L.N. Savushkin, Phys. Rev. C **48**, 2665 (1993).
[13] B. ter Haar and R. Malfliet, Phys. Rep. **149**, 207 (1987).
[14] H. Müther, R. Machleidt, and R. Brockmann, Phys. Lett. B **202**, 483 (1988); Phys. Rev. C **42**, 1981 (1990).
[15] R. Fritz, H. Müther, and R. Machleidt, Phys. Rev. Lett. **71**, 46 (1993).
[16] R. Brockmann and H. Toki, Phys. Rev. Lett. **68**, 3408 (1992).
[17] S. Haddad and M.K. Weigel, Phys. Rev. C **48**, 2740 (1993).
[18] S. Gmuca, J. Phys. G **17**, 1115 (1991); Z. Phys. A **342**, 387 (1992); Nucl. Phys. **A547**, 447 (1992).
[19] J. Boguta and J. Rafelski, Phys. Lett. B **71**, 22 (1977).
[20] F.E. Serr and J.D. Walecka, Phys. Lett. B **79**, 10 (1978).
[21] B.D. Serot and J.D. Walecka, Phys. Lett. B **87**, 172 (1979).
[22] C.J. Horowitz and B.D. Serot, Nucl. Phys. **A368**, 503 (1981).
[23] W. Stocker and M.M. Sharma, Z. Phys. A **339**, 147 (1991).
[24] D. Von-Eiff, J.M. Pearson, W. Stocker, and M.K. Weigel, Phys. Lett. B **324**, 279 (1994).
[25] C. Speicher, E. Engel, and R.M. Dreizler, Nucl. Phys. **A562**, 569 (1993).
[26] M. Centelles and X. Viñas, Nucl. Phys. **A563**, 173 (1993).
[27] D. Hofer and W. Stocker, Nucl. Phys. **A492**, 637 (1989). (The convergence problems for the nonlinear case have been solved.)
[28] M.M. Sharma, M.A. Nagarajan, and P. Ring, Phys. Lett. B **312**, 377 (1993).
[29] R. Machleidt, Adv. Nucl. Phys. **19**, 189 (1989).
[30] W.D. Myers and W.J. Swiatecki, Ann. Phys. (N.Y.) **55**, 395 (1969).
[31] W.D. Myers, Nucl. Phys. **A204**, 465 (1973).
[32] G. Süßmann, Z. Phys. A **274**, 145 (1975).
[33] M. Farine, J. Côté, and J.M. Pearson, Nucl. Phys. **A338**, 86 (1980).
[34] D. Von-Eiff and M.K. Weigel, Phys. Rev. C **46**, 1797 (1992).
[35] W. Stocker, Phys. Lett. B **104**, 339 (1981).
[36] C. W. de Jager, H. de Vries, and C. de Vries, At. Data Nucl. Data Tables **14**, 479 (1974).
[37] H. de Vries, C. W. de Jager, and C. de Vries, At. Data Nucl. Data Tables **36**, 495 (1987).
[38] A.R. Bodmer and C.E. Price, Nucl. Phys. **A505**, 123 (1989).
[39] M. Centelles, X. Viñas, M. Barranco, S. Marcos, and R.J. Lombard, Nucl. Phys. **A537**, 486 (1992).
[40] M.A. Thorpe and D.J. Thouless, Nucl. Phys. **A156**, 225 (1970).
[41] C.E. Price, J.R. Shepard, and J.A. McNeil, Phys. Rev. C **41**, 1234 (1990).
[42] W. Stocker, Nucl. Phys. **A140**, 305 (1970); **A159**, 222 (1970).
[43] M. Brack, C. Guet, and H.-B. Håkansson, Phys. Rep. **123**, 275 (1985).
[44] M. Durand, P. Schuck, and X. Viñas, Z. Phys. A **346**, 87 (1993).